

Received May 24, 2021, accepted June 12, 2021, date of publication June 15, 2021, date of current version June 22, 2021.

Digital Object Identifier 10.1109/ACCESS.2021.3089637

Type Synthesis and Kinematic Analysis of a 2-DOF Shape-Morphing Wheel Mechanism for Step-Overcoming

YOUNGSOO KIM¹, HWA SOO KIM², (Member, IEEE),
AND TAEWON SEO³, (Senior Member, IEEE)

¹School of Mechanical and Aerospace Engineering, Seoul National University, Seoul 08826, South Korea

²Department of Mechanical System Engineering, Kyonggi University, Suwon 16227, South Korea

³School of Mechanical Engineering, Hanyang University, Seoul 04763, South Korea

Corresponding authors: Hwa Soo Kim (hskim94@kgu.ac.kr) and TaeWon Seo (taewonso@hanyang.ac.kr)

This work was supported in part by the Basic Science Research Program through the National Research Foundation of Korea Grant by the Ministry of Education under Grant NRF-2019R1A2C1008163, in part by the Gyeonggi-do Regional Research Center (GRRC) Program of Gyeonggi Province through the Research on Innovative Intelligent Manufacturing Systems under Grant GRRC KGU 2021-B02, and in part by the Korea Agency for Infrastructure Technology Advancement (KAIA) Grant by the Ministry of Land, Infrastructure and Transport under Grant 21CTAP-C164242-01.

ABSTRACT This study presents a novel shape-morphing wheel that enables to not only traverse flat ground quickly in a circular configuration but also overcome obstacles like steps effectively in a transformed configuration. The proposed wheel mechanism has two degrees-of-freedom (DOFs) to change its wheel radius and the tilting angle of its lobe simultaneously in response to obstacles of various sizes. The kinematic requirements for the 2-DOF shape-morphing wheel mechanism are first defined. Then, the proper mechanisms for the proposed wheel mechanism are exhaustively searched. As a result, five mechanisms are selected in combination with four-bar mechanism to synchronize the motions of wheel lobes. From the kinematic viewpoints including the singularity, transformation range and interference, the characteristics of selected mechanisms are analyzed extensively, and a novel 2-DOF shape-morphing wheel mechanism has been successfully constructed.

INDEX TERMS Kinematics, mobile platform, shape-morphing, step-overcoming, type synthesis.

I. INTRODUCTION

In order to perform various tasks such as guidance, healthcare and surveillance, indoor service robots should be able to move around human living environments quickly and safely. From this viewpoint, a wheel is an effective mechanism for robots to traverse flat ground because of its simple structure, high efficiency, and smooth motion even at high speeds. Most recent service robots are based on wheel mechanisms; for example, T-Rot [1], HealthBot [2], May [3], Fetch and Freight [4], HSR [5].

However, conventional wheeled robots have the difficulty in overcoming structured obstacles such as steps and stairs, which are frequently encountered in indoor environments [6]. In general, the maximum height of a step that a conventional wheeled robot can overcome is known equal to the radius of

its wheel [7]. With respect to steps and stairs without vertical surfaces (called as risers), a wheeled robot's overcoming ability becomes considerably deteriorated owing to the lack of friction. Furthermore, although the wheel mechanism can overcome small steps or stairs, it may undergo dynamic impact at high speeds and, in the worst scenario, may even fall down from the steps or stairs [8]. Therefore, to overcome steps and stairs effectively, a wheeled robot must have a reliable way to maintain good contact with these structured obstacles.

Over the last decades, many studies have been conducted to provide the appropriate ability for wheel mechanisms to overcome obstacles without compromising their advantages. For example, legged wheels have been proposed to ensure fast movement on a plane and high adaptability against various stairs. Among wheel-legged mechanisms, RHex is the most famous robot; with the help of six half-circle spokes, it can overcome various obstacles in indoor and outdoor

The associate editor coordinating the review of this manuscript and approving it for publication was Wai-Keung Fung¹.

environments [9]. However, the irregularity of its rotational radius may cause periodic oscillations, which may be a hurdle in performing various indoor tasks. To improve the mobility of legged wheel mechanisms on a plane, circular wheels have been added to the ends of their spokes; for example, a two wheel-legged compact mechanism, Ascento, has been designed for indoor inspection task. However, it still has the problem to overcome stairs successively because its basic function to overcome obstacles is jumping [10].

To resolve the undesired discontinuity observed in the locomotion of legged wheels, reconfigurable wheels have been explored, whose degrees-of-freedom (DOF) is increased by adopting a proper mechanism, in other words, their shapes can be transformed from the conventional circle to the legged shape. For example, the Wheel Transformer can passively change its wheel shape from a circle to a legged shape. As a result, it can overcome an obstacle of 150 mm in height (twice the diameter of the wheel). However, the Wheel Transformer requires a vertical riser to trigger its wheel transformation, and it cannot climb stairs in a smooth manner [11]. To the contrary, the wheels of a Quattroped can be converted into semi-circular wheels by actively folding them in half [12]. Different from the Wheel Transformer, the Quattroped utilizes two actuators for wheel transformation, but it must stop completely twice for wheel transformation and alignment before overcoming obstacles. Recently, this defect has been addressed by redesigning the leg-wheel transformation mechanism so that the TurboQuad does not require the rest mode during its wheel transformation [13]. It is worthwhile to note that because the transformed shapes of existing reconfigurable wheels are uniquely fixed, the sizes of the steps and stairs that the mobile robots equipped with reconfigurable wheels can climb are inevitably limited. To increase the adaptability of mobile robots to various steps and stairs, soft materials have been recently adopted for their wheels using the origami method [14], [15].

Wheel-linkage design is a viable candidate for locomotion on uneven and structured surfaces, including steps and stairs. The well-known rocker-bogie mechanism has been chosen as the base platform for space rovers such as Spirit, Opportunity, and Curiosity [16]. In the Shrimp mechanism, a front fork is added to the bogie to improve the climbing ability of the rocker-bogie. As a result, it can climb a step whose height is twice the wheel diameter [17]. Certain studies based on the rocker-bogie and Shrimp mechanisms have been conducted for stair climbing. A novel mechanism has been proposed that combines tracks with wheels using linkages to ensure climbing ability for stairs of various sizes [6], [18]. Whereas the rocker-bogie and Shrimp mechanisms are based on passive links, wheel-linkage based wheelchairs use multiple active links to guarantee their mobile stability and good capability to overcome obstacles [19]. Therefore, their structures become complicated, and their climbing motions are typically slower because of the complexity of sensing and control. In [20], the Stewart platform based wheel-linkage robot is proposed to ensure a higher load capacity and more flexible

behavior in various environments in comparison with existing wheel-legged mechanisms. In general, wheel-linkage solutions exhibit high adaptability against stairs and stable locomotion on the ground, but their stair-climbing speeds remain unsatisfactory.

In this study, we propose a novel 2-DOF shape-morphing wheel that can move on flat ground quickly and overcome various obstacles in indoor environments efficiently. Because the proposed shape-morphing wheel comes in contact with only the horizontal surface of the obstacle, the absence of a vertical riser of the obstacle has no influence on the climbing performance of a mobile robot equipped with the proposed wheels. In addition, it is possible to overcome various obstacles in indoor environments more smoothly via the continuous transformation of proposed 2-DOF wheel. Herein, various mechanisms have been explored for the novel 2-DOF shape-morphing wheel. Since the serial two-bar and parallel five-bar mechanisms basically have a 2-DOF motion, they are considered as the possible candidates for the proposed 2-DOF wheel with different combinations of revolute and prismatic joints. Then, their kinematic properties have been exhaustively analyzed to choose the proper mechanism that can satisfy the requirements for the given task. In other words, we examine whether the selected wheel mechanism can be changed into the desired shape, whether the interferences between its links or between its links and an obstacle occur while overcoming the obstacle, and whether more than two passive revolute joints are arranged in a row. Recall that if more than two passive revolute joints are arranged in a row, the transformation of the wheel mechanism is highly restricted owing to the singularity and as a result, it is likely to fail to change its shape appropriately against an obstacle.

The remainder of this paper is organized as follows. Section 2 describes the concepts and kinematic requirements for the 2-DOF shape-morphing wheel. In Section 3, the 2-DOF shape-morphing mechanisms are systematically investigated through the type synthesis of two- and five-bar mechanisms. By excluding candidates that does not satisfy the kinematic conditions and incorporating the synchronizing mechanism, five mechanisms are derived. In Section 4, the kinematic characteristics of five mechanisms are analyzed by using the transformation range, interference, singularity, etc. The concluding remarks are presented in Section 5.

II. 2-DOF SHAPE-MORPHING WHEEL

A. CONCEPT OF THE SHAPE-MORPHING WHEEL

The kinematic structure of the proposed 2-DOF shape-morphing wheel, which consists of three wheel spokes and three wheel lobes, is presented in Fig. 1. In Fig. 1, r , θ , and φ denote the wheel radius from the wheel center to the hinge joint of the lobe, the tilting angle of the lobe with respect to the wheel spoke, and the rotating angle of the wheel center, respectively. In this study, the proposed wheel has two DOFs for transformation along the r - and θ -directions; in other words, the wheel radius and tilting angle of the

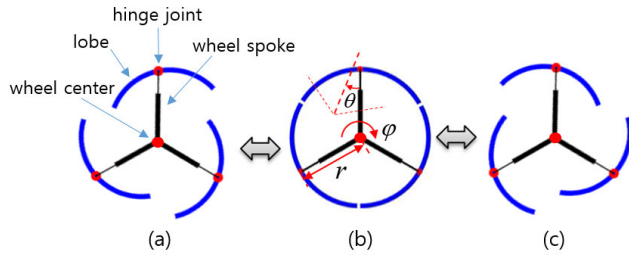


FIGURE 1. Design parameters of the 2-DOF shape-morphing wheel and its shapes: (a), (c) bi-directional shape for obstacle overcoming and (b) circular shape for locomotion on flat ground.

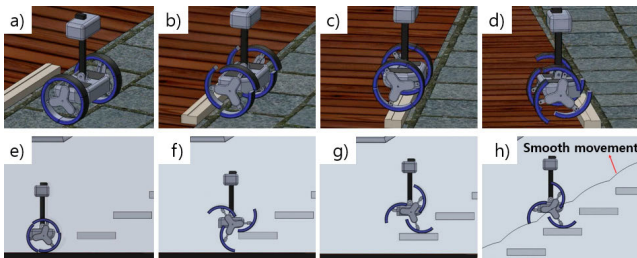


FIGURE 2. Two examples of the proposed wheel overcoming obstacles encountered in indoor environments: (a)–(d) overcoming a step and (e)–(h) overcoming stairs.

lobe can be changed within certain ranges. To guarantee the lightness of the proposed wheel, an appropriate mechanism is integrated to synchronize the tilting motions of the three wheel lobes such that only two actuators are used for the desired transformation of the proposed wheel. Unlike fixed 1-DOF transformations of the Wheel Transformer and Quat-troped, the proposed wheel is characterized by its continuous transformability, which significantly enhances its prompt adaptability against obstacles of various sizes.

Fig. 2 presents two examples of a mobile robot with the proposed shape-morphing wheel, where it overcomes a step and stairs in an indoor environment. While overcoming the step, as shown in Figs. 2(a)–(d), the proposed wheel is able to arbitrarily rotate its lobes in the clockwise and counter-clockwise directions such that the mobile robot can effectively change its moving direction on the spot, without steering. In fact, stair-overcoming is equivalent to successive step-overcoming as shown in Figs. 2(e)–(h); however, it is important to reduce unexpected fluctuations of the mobile robot to prevent it from falling from a stair. Hence, the trajectory of the wheel center must be sufficiently smoothed, which may be possible using optimal trajectory planning, accompanied by proper wheel transformation to the size and shape of the given stair [21].

Fig. 3 shows the sequential stages in step-overcoming using the proposed shape-morphing wheel, where l and h denote the circumference of the wheel lobe and height of the step, respectively, and α and β correspond to the lengths of the ground that are not touched by the wheel lobe before the next wheel lobe touches the upper ground of the step. The pre-transformation of the wheel at the second stage can

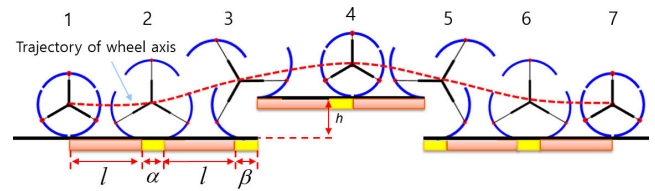


FIGURE 3. Sequential stages in step-overcoming using the proposed 2-DOF shape-morphing wheel.

TABLE 1. Key requirements For 2-DOF Shape-morphing wheel.

K1	The diameter of circular wheel is less than 260 mm
K2	The DOF of shape-morphing wheel is two
K3	The motions of all wheel lobes are synchronized
K4	All parts of mechanism are located inside the proposed wheel
K5	The proposed wheel has the adaptability to various obstacles
K6	There is no interference between wheel and environments
K7	The minimum torque required to overcome obstacles becomes smaller
K8	The structural stiffness is sufficiently ensured
K9	The accuracy of wheel transformation is ensured
K10	The structure of proposed wheel becomes simple
K11	The proposed wheel is fabricated easily

determine the optimal values of α and β to not only make the trajectory of the wheel center much smoother but also make the correct contact at the third stage. In addition, for descending a step at the fifth stage, the shape of the transformed wheel is axially symmetric with respect to that for climbing a step at the third stage.

B. REQUIREMENTS FOR THE SHAPE-MORPHING WHEEL

To determine the proper 2-DOF shape-morphing wheel mechanism, the key requirements that the proposed wheel must satisfy are defined and summarized in Table 1. First, the requirement **K1** sets the limit on the wheel size. A larger wheel size may offer improved performance in terms of overcoming obstacles; however, in this study, we set a limit on the wheel size because the minimum length of the tread of the stair is 260 mm [22]. Therefore, the radius of the proposed wheel in the circular shape is chosen to be 125 mm, such that with three wheel lobes, the length of one lobe would be less than 260 mm. The requirements **K2** and **K3** are related to the kinematic structure of the proposed shape-morphing wheel. As discussed in Section 2.A, the total DOF of the proposed wheel is selected to be two, i.e., one DOF for the length change of the wheel spoke and the other DOF for rotation of

the wheel lobe. In combination with a mechanism to synchronize the motions of all the wheel lobes, only two actuators are used for the 2-DOF wheel transformation. The requirements **K4–K6** are related to the basic requirements that the shape-morphing wheel must satisfy to overcome obstacles. The requirements **K7–K11** are considered to determine the proper mechanism for the 2-DOF wheel mechanism.

To derive various shapes of the proposed wheel for the requirement **K5**, the sizes of the obstacles should be defined. Various obstacles may be encountered in the human living environment, and most of them consist of a combination of vertical and horizontal surfaces, similar to steps and stairs. According to the Building Code [22], the width of a public stairway must be at least 260 mm, and the height must be less than 200 mm. When the initial posture and position of the proposed wheel are given, i.e., (r, θ) is fixed, the distance between the wheel and a step S (equal to the tread length) and the height of the step H can be determined using the kinematic relation shown in Fig. 4(a) as follow:

$$S = \left(\theta_2 - \frac{\sqrt{3}}{2}\right) r_2 + \{\sin \theta - \sin(\theta - \theta_2)\} r \quad (1)$$

$$H = -\frac{\sqrt{3}}{2} r_2 + \{\cos(\theta - \theta_2) - \cos \theta\} r \quad (2)$$

where r_2 is selected to be 125 mm based on the requirement **K1** and $\theta_2 = \frac{2\pi}{3}$ because the number of wheel lobes is chosen to be three for the structural simplicity of the proposed wheel. The required transformation ranges of the length of the wheel spoke r and tilting angle of the wheel lobe θ are presented in Fig. 4(b), where $260 \text{ mm} \leq S \leq 340 \text{ mm}$ and $|H| \leq 200 \text{ mm}$. The negative sign of H implies that the proposed wheel climbs down a step with a tread and height of $S \times |H| \text{ mm}^2$. As confirmed in Fig. 4(b), as the tread length increases with constant height (from **P3** to **P4** or from **P6** to **P7**), the required transformation range of the wheel spoke increases, but the required range of the tilting angle of the lobe decreases. In contrast, as the height of the step increases with constant tread length, the required ranges of the wheel spoke and tilting angle of the lobe increase simultaneously. In summary, for the given ranges of S and H in Fig. 4(b), the required ranges of the wheel spoke and tilting angle of the lobe were from 125 mm to 205.6 mm and from -43° to 43° , respectively.

III. TYPE SYNTHESIS OF THE 2-DOF SHAPE-MORPHING WHEEL

A. 2-DOF MECHANISMS

In this study, we adopt the type synthesis method to find the proper mechanism for achieving a 2-DOF motion of three lobes that can satisfy the kinematic requirements in Table 1. First, we explore various 2-DOF kinematic structures to transform the position and posture of the wheel lobe with respect to the wheel base. According to Gruebler's equation, the 2-DOF mechanisms with the smallest number of links and joints are serial 2-DOF mechanisms. Because there are only two joints, both the joints must be active joints. As shown in

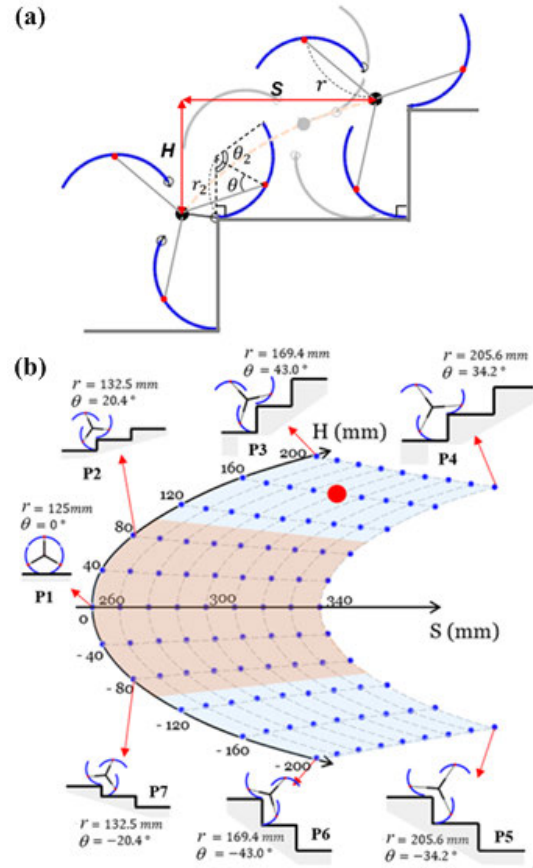


FIGURE 4. (a) Kinematic relation between the proposed wheel and a step during step-overcoming and (b) required transformation ranges of length of wheel spoke r and tilting angle of wheel lobe θ .

Fig. 5, according to the combination of revolute joint **R** and prismatic joint **P**, there are four cases, (1)–(4).

Next, a parallel mechanism consisting of five links and five joints is considered as another candidate. In this case, two joints are active joints, and three joints are passive joints. Note that the active joints must be supported by the base. According to the combination of **R** and **P**, there are thirty-two kinematic structures, as shown in Fig. 5 considering that the mirror-symmetric mechanism is the same as the original mechanism.

As shown in Fig. 5, a detailed investigation of mechanisms is required to check whether the key requirements listed in Table 1 are satisfied or not. To streamline the design procedure of the 2-DOF shape-morphing wheel, we first analyze the motion of the mechanism with passive prismatic joints (for example, (10) **RPRRR** in Fig. 5). For the linear motion of the passive prismatic joint, a linear guide is essential, which has a sufficient stroke to meet the required transformation range in Fig. 4(b). Moreover, active prismatic joints are preferred because passive prismatic joints tend to cause problems related to friction and accuracy [23]. In this **RPRRR** mechanism, the rotation of each actuator must be changed into a passive linear motion of the prismatic joint, and a normal force perpendicular to the linear motion of

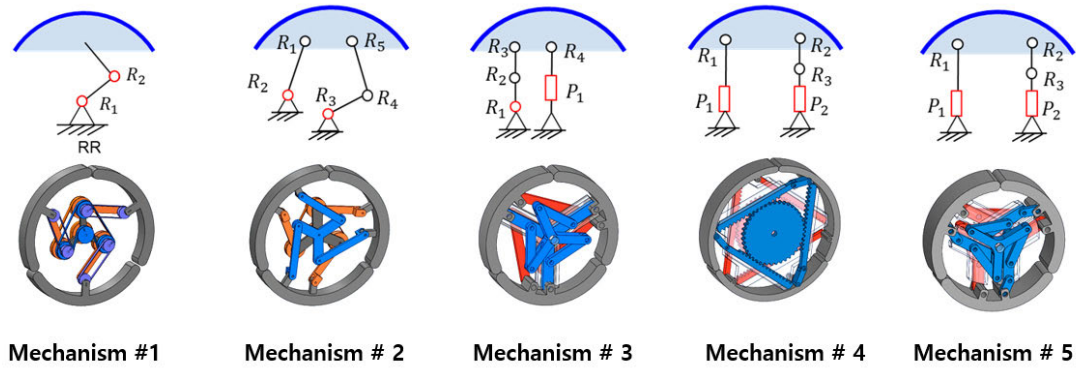


FIGURE 6. Five mechanisms combined with the synchronization mechanisms for the 2-DOF shape-morphing wheel mechanism.

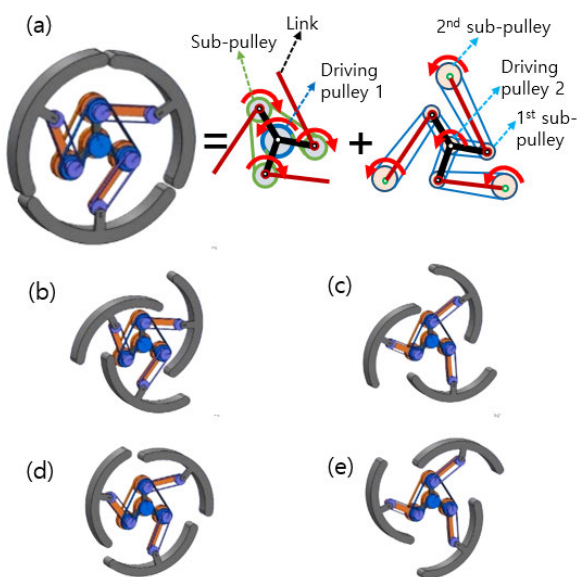


FIGURE 7. (a) Mechanism #1 combined with two pairs of pulley mechanisms for the 2-DOF shape-morphing wheel mechanism, and (b), (c), (d), and (e) its transformed shapes according to the combined rotations of pulley 1 and 2.

where q_1 denotes the joint angle between the fixed link and Link. Fig. 8(b)–(c) show that with an appropriate choice of design parameters, mechanism #1 can be transformed into desired shapes whose radius and tilting angle of the lobe are within the desired transformation ranges. However, the motions of the links and lobes obtained by two pulley mechanisms are highly coupled to each other; for example, when the joint **R1** rotates by the orange belts, the joint **R2** rotates by the revolution of the pulley located at joint **R2**. Therefore, the positioning and angle accuracy of its transformed shape are likely to suffer from accumulated errors, and the required torques becomes increased because all the active joints are rotational. Recall that joint **R1** must be within a circle with a radius of 62 mm, as shown in Fig. 8(a), to avoid undesired interference between links during its transformation; hence, the maximum length of l_1 is set to 62 mm. The minimum radius of the circular shape is 125 mm.

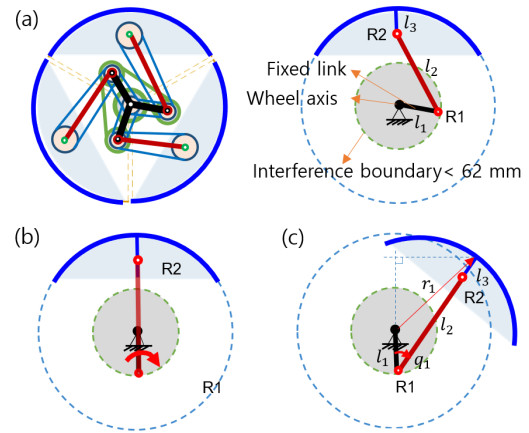


FIGURE 8. (a) Design parameters of mechanism #1, (b) and (c) a configuration to maximize the radius of its transformed shape.

2) MECHANISM #2

Mechanism #2 is based on a parallel five-bar structure, and all the joints are composed of revolute joints. The motions of the three lobes are synchronized by the combination of a belt-pulley mechanism and a ternary link rotating with respect to the wheel axis, as shown in Fig. 9(a). Figs. 9(b)–(e) present four transformed shapes of mechanism #2 according to the combined rotations of the belt-pulley and ternary link. The transformed shapes in Figs. 9(b) and 9(c) are obtained by the counter-clockwise rotations of the ternary link and driving pulley, respectively. The transformed shapes in Figs. 9(d) and 9(e) are obtained by the combination of the counter-clockwise rotation of the driving pulley and ternary link. Similar to mechanism #1, the motions of the pulley and ternary links of mechanism #2 are highly coupled to each other.

3) MECHANISM #3

Mechanism #3 is a 4 **R1P** mechanism, with one **P** joint in the wheel base, as shown in Fig. 10(a). The motions of the three lobes are synchronized by a combination of two pairs of ternary links rotating with respect to the wheel axis. Figs. 10(b)–(e) present four transformed

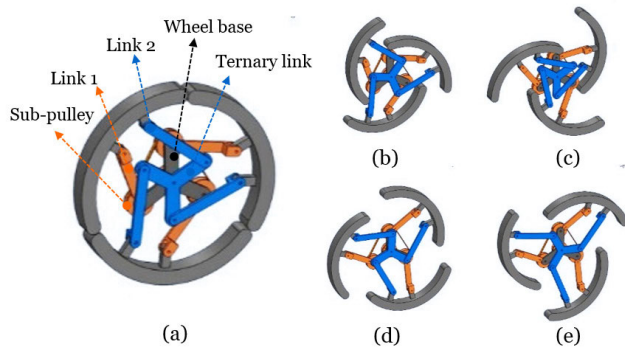


FIGURE 9. (a) Mechanism #2 combined with a belt-pulley mechanism and ternary link for the 2-DOF shape-morphing wheel mechanism, and (b), (c), (d), and (e) its transformed shapes according to the combined rotations of the pulley and ternary link.

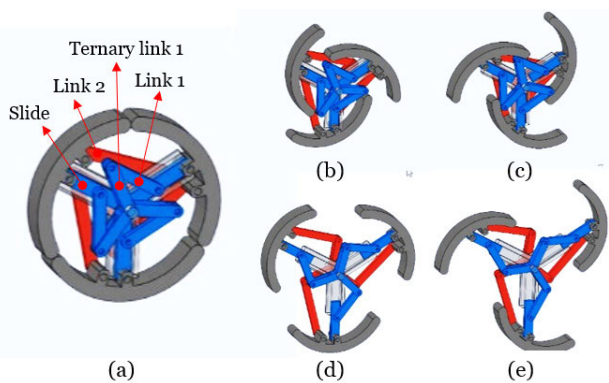


FIGURE 10. (a) Mechanism #3 combined with two pairs of ternary links for the 2-DOF shape-morphing wheel mechanism, and (b), (c), (d), and (e) its transformed shapes according to the combined rotations of ternary links.

shapes of mechanism #3 according to the combined rotations of the two ternary links. The transformed shapes in Figs. 10(b) and 10(c) are obtained by the counter-clockwise rotation of the red ternary link and the clockwise rotation of the blue ternary link, respectively. The transformed shapes in Fig. 10(d) and 10(e) are obtained by the combination of the counter-clockwise rotation of the red ternary link and clockwise rotation of the blue ternary link.

4) MECHANISM #4

Mechanism #4 is a 3 **R2P** mechanism, with two **P** joints in the wheel base, as shown in Fig. 11(a). All **P** joints are driven by a rack-pinion mechanism. If the stroke lengths of the two **P** joints are equal, the deformation occurs only along the r -direction. Otherwise, the wheel lobe rotates proportionally to the difference between the two stroke lengths. Figs. 11(b)–(e) present four transformed shapes of mechanism #4 according to the combined translations of two rack-pinions. The transformed shapes in Figs. 11(b) and 11(c) are obtained by the clockwise rotation of the blue pinion and the counter-clockwise rotation of the red pinion, respectively. The transformed shapes in Fig. 11(d) and 11(e) are obtained by the combination of the clockwise and counter-clockwise

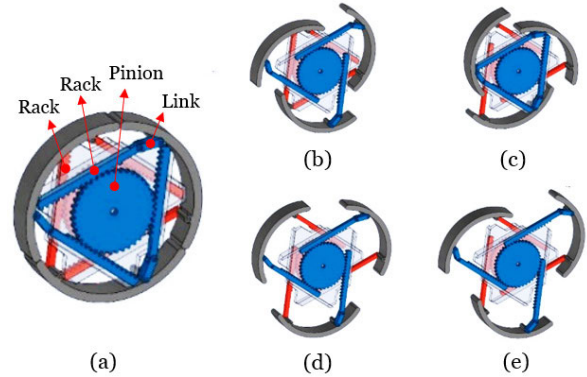


FIGURE 11. (a) Mechanism #4 combined with two pairs of rack-pinions for the 2-DOF shape-morphing wheel mechanism, and (b), (c), (d), and (e) its transformed shapes according to the combined rotations of the rack-pinions.

rotations of the blue and red pinions. To prevent interference between lobes, the length of the rack and resulting stroke must be limited. The size of the pinion is equal to the circle tangent to the three racks.

5) MECHANISM #5

Mechanism #5 is a 3 **R2P** mechanism, with two **P** joints in the wheel base, as shown in Fig. 12(a). Actually, mechanism #5 is similar to mechanism #4, except for the connecting mechanism for the lobe. When compared to mechanism #4, whose stroke is limited by the rack-pinion, mechanism #5 has a larger stroke because the prismatic slide is attached to the radial direction of the wheel. Figs. 12(b)–(e) present four transformed shapes of design alternative #5 according to the combined rotations of the two ternary links. The transformed shapes in Figs. 12(b) and 12(c) are obtained by the counter-clockwise rotation of the red ternary link and the clockwise rotation of the blue ternary link, respectively. The transformed shapes in Figs. 12(d) and 12(e) are obtained by the combination of the clockwise and counter-clockwise rotations of the blue and red ternary links.

IV. SIMULATION AND PERFORMANCE EVALUATION OF FIVE SELECTED MECHANISMS

A. SIMULATION CONDITIONS AND RESULTS

To determine the proper mechanism for the 2-DOF shape-morphing wheel mechanism among the five mechanisms, a simulation to climb up/down a step is conducted to compare the performances of five selected mechanisms. As shown in Fig. 13, it is assumed that the height of the step is 180 mm, and the distance between the design alternative and the step is set to 780 mm. As discussed in the previous section, the radius of the design alternative in a circular shape is 125 mm.

Based on our previous study on the trajectory planning of a transformable wheel [21], the trajectory of the wheel center can be determined by an appropriate wheel transformation to minimize undesired fluctuations during it step-overcoming. Fig. 14 presents the desired objective trajectories of wheel radius r and tilting angle of the lobe θ . As shown in Fig. 14,

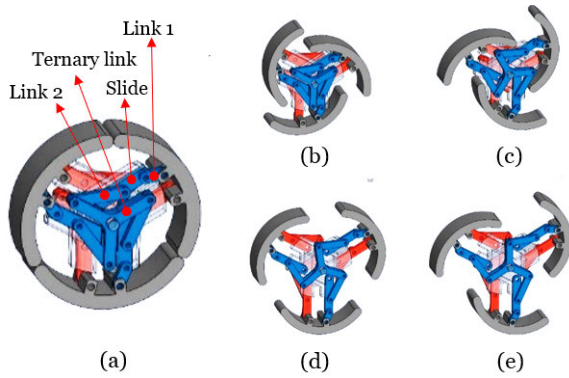


FIGURE 12. (a) Mechanism #5 combined with two pairs of ternary links for the 2-DOF shape-morphing wheel mechanism, and (b), (c), (d), and (e) its transformed shapes according to the combined rotations of two ternary links.

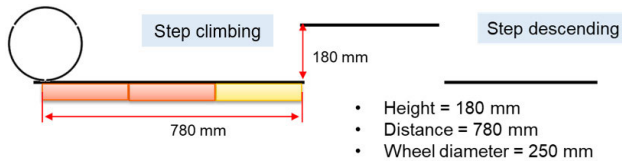


FIGURE 13. Conditions of the step-overcoming simulation.

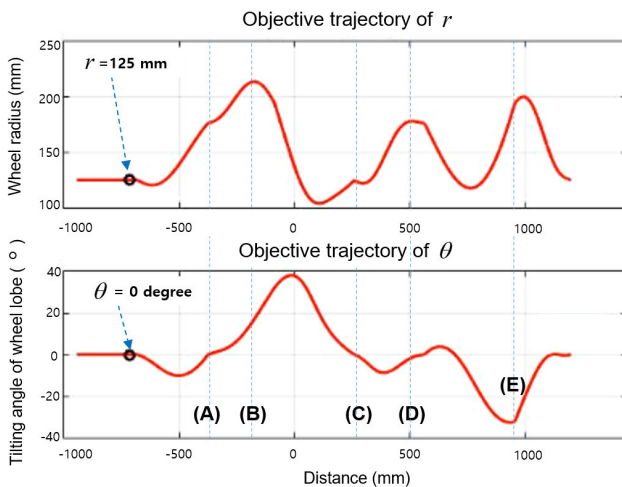


FIGURE 14. Objective trajectories of the wheel radius and the tilting angle of wheel lobe for smooth step-overcoming, which is obtained using optimal trajectory planning [21].

the wheel radius gradually increases at (A) to reduce the distance between the end point of the lobe contacting the ground and the step less than the circumference of the wheel lobe. This occurs without a change in the tilting angle of the lobe for smooth obstacle overcoming, which corresponds to the second stage in Fig. 3. Then, the radius becomes maximum at (B) to climb up the step by increasing the tilting angle of the lobe, which corresponds to the third stage in Fig. 3. After climbing up the step, its shape is transformed into a circular shape at (C). When transforming from (C) to (D), the wheel radius changes similar to (A), without changing the tilting angle of the lobe. Finally, the wheel radius increases

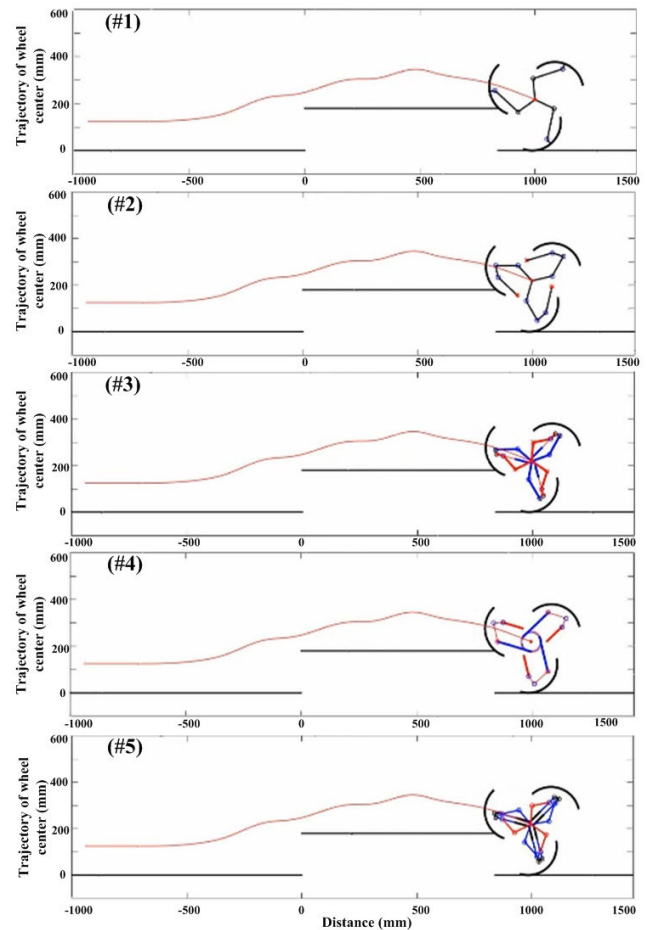


FIGURE 15. Objective trajectories of the wheel radius and the tilting angle of wheel lobe for smooth step-overcoming, which is obtained using optimal trajectory planning [21].

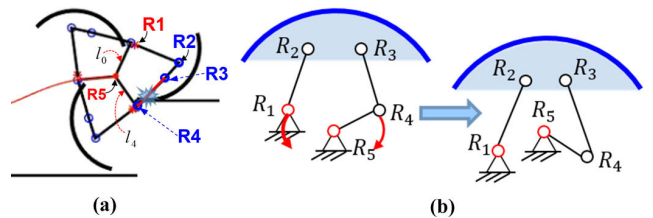
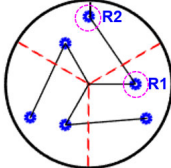
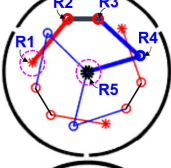
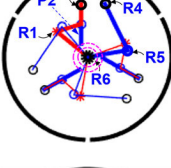
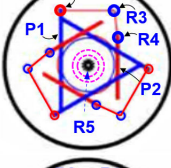
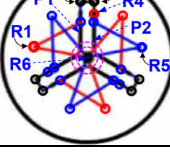


FIGURE 16. (a) Interference between the corner of the step and link connecting joints R3 and R4 and (b) final configuration of mechanism #2.

again, but the tilting angle of the wheel lobe decreases at (E) to descend the step, which corresponds to the fifth stage in Fig. 3. The tilting angle of the wheel lobe for climbing an obstacle is opposite to that for descending it, as previously shown in Fig. 3.

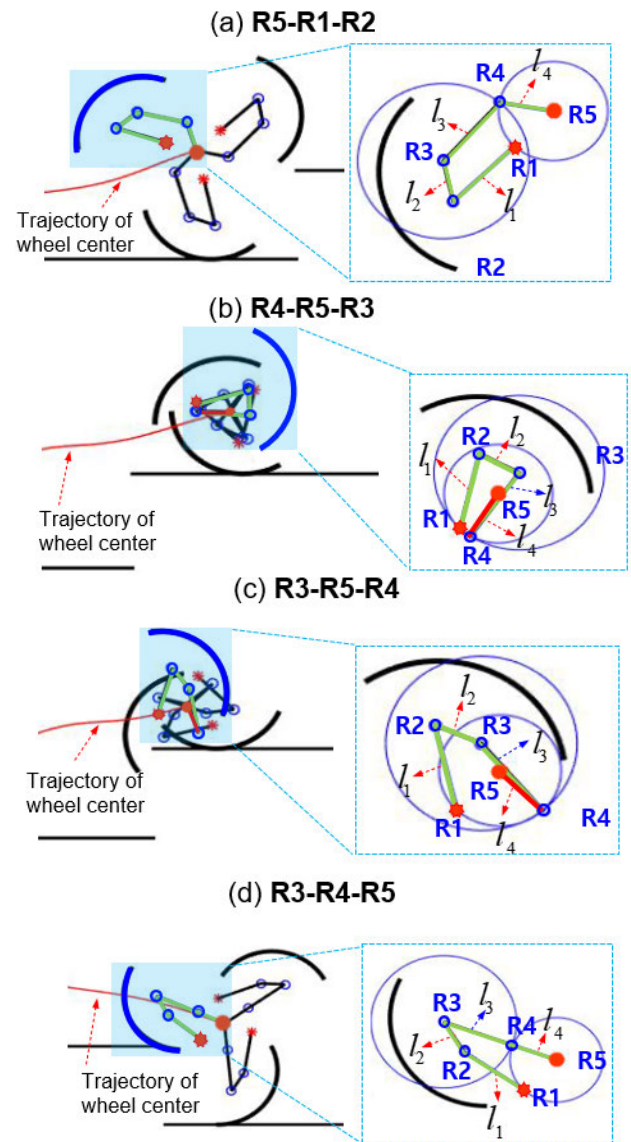
For the given objective trajectories of the wheel radius and tilting angle of the lobe in Fig. 14, the joint variables for each mechanism are numerically calculated through geometric analysis. Table 2 summarizes the initial parameters of each mechanism used for the step-overcoming simulation with respect to the center (0, 0) of their rotations, where the

TABLE 2. Initial parameters of five mechanisms for step-overcoming simulation.

	Kinematic structure	Joint location
Mechanism #1		$R1 = (42, -50)$ $R2 = (0, 90)$
Mechanism #2		$R1 = (-15, -90)$ $R2 = (-25, 80)$ $R3 = (25, 80)$ $R4 = (10, 90)$ $R5 = (0, 0)$
Mechanism #3		$R1 = (-52, 30)$ $P2x = -10$ $R3 = (-10, 80)$ $R4 = (10, 80)$ $R5 = (52, 30)$ $R6 = (0, 0)$
Mechanism #4		$P1x = -40, P2x = 45$ $R2 = (-40, 80)$ $R3 = (40, 80)$ $R4 = (40, 40)$ $R5 = (0, 0)$
Mechanism #5		$P1x = -10, P2x = 10$ $R1 = (-78.78, 13.89)$ $R2 = (-15, 80)$ $R3 = (10, 80)$ $R4 = (10, 60)$ $R5 = (78.78, 13.89)$ $R6 = (0, 0)$

active joints are denoted by magenta circles. The mechanisms in Table 2 are equipped with an appropriate synchronization mechanism for the corresponding three lobes to produce the same motion; hence, their shapes in Table 2 may seem to be different from the simple shapes shown in Fig. 5 or at the top of Fig. 6. It is worthwhile to note that through the simulations, the joint variables of each mechanism may be adjusted as required to prevent interference and singularities.

Then, the simulation is performed, where each mechanism climbs up and down the step, as shown in Fig. 13, while the wheel radius and tilting angle of the wheel lobe track the objective trajectories, as shown in Fig. 14. In Fig. 15, the center trajectories of each design alternative are denoted by a red line. Recall that the objective trajectories of the wheel radius and tilting angle of the wheel lobe are derived from the optimal trajectory of the wheel center studied in [21]; therefore, the resulting trajectories of the wheel centers of all the mechanisms are the same, as confirmed in Fig. 15. However, because their structures are different from each other, the corresponding motions of their joints and links are different. As a result, for certain mechanisms, undesired phenomena such as interference between links and step

**FIGURE 17.** Singular conditions of mechanism #2: (a) when joints R5, R1, and R2 are located in a straight line, (b) when joints R4, R5, and R3 are located in a straight line, (c) when joints R3, R5, and R4 are located in a straight line, and (d) when joints R3, R4, and R5 are located in a straight line.

and singularities are observed, which are discussed in detail in the next section. For more information on the simulation, please refer to the attached video files of five selected mechanisms.

B. ANALYSIS AND PERFORMANCE EVALUATIONS

1) MECHANISM #2

During the step-overcoming simulation shown in Fig. 15, it is observed that mechanism #2 suffers from undesired interference between the corner of the step and its link connecting joints R3 and R4, which occurs before mechanism #2 starts to climb up the step, as shown in Fig. 16(a). For this type of interference, joints R1 and R4 must be within a circle with a radius of 60 mm from joint R5. Furthermore, mechanism #2

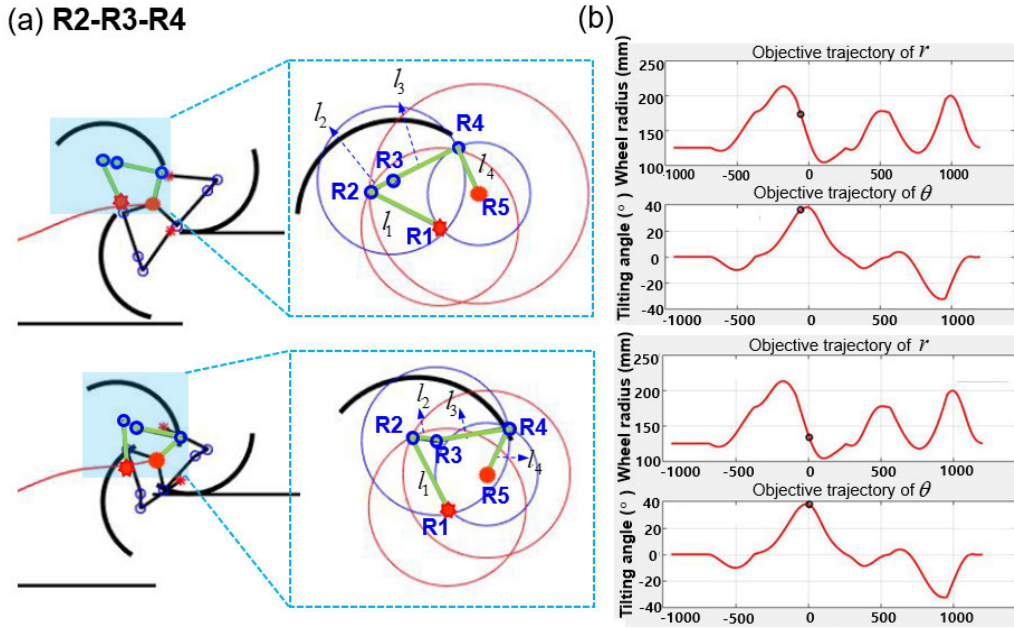


FIGURE 18. (a) Another singular condition of mechanism #2: when joints R2, R3, and R4 are located in a straight line and (b) corresponding wheel radius and tilting angle of the wheel lobe.

should satisfy the required transformation range described in Fig. 4(b). Thus, two lengths $l_0 + l_1$ and $l_3 + l_4$ must be increased, and the final configuration of this mechanism is derived, as shown in Fig. 16(b).

The singularity of mechanism #2 is further investigated for the given configuration in Fig. 16(b). In this mechanism, the singularity may occur when three revolute joints are located in a straight line. Then, there is a strong restriction on the transformation of the mechanism. There are four cases in which singularity occurs while mechanism #2 climbs up and down the step. For example, if joints R2, R1, and R5 are in a straight line, as shown in Fig. 17(a), the radius of mechanism #2 can be increased no longer. Further, if R4, R5, and R3 are in a straight line as shown in Fig. 17(b), the radius of mechanism #2 cannot be decreased. In the case shown in Fig. 17(c), the tilting angle of mechanism #2 cannot be decreased. In these types of singularities, the position and tilting angle of each lobe can be achieved by appropriately manipulating active joints R1 and R5; thus, the inverse kinematics of mechanism #2 can be solved such that all joint values are uniquely determined. To avoid these singularities, the following conditions must be satisfied:

$$\begin{cases} d(\mathbf{R5} - \mathbf{R2}) \leq d(\mathbf{R5} - \mathbf{R1}) + d(\mathbf{R1} - \mathbf{R2}) \\ d(\mathbf{R5} - \mathbf{R2}) \geq d(\mathbf{R5} - \mathbf{R1}) - d(\mathbf{R1} - \mathbf{R2}) \\ d(\mathbf{R5} - \mathbf{R2}) \geq d(\mathbf{R1} - \mathbf{R2}) - d(\mathbf{R5} - \mathbf{R1}) \end{cases} \quad (4)$$

where $d(\cdot)$ denotes the distance between two points. Eq. (4) can be expressed as

$$|l_1 - l_2| \leq d(\mathbf{R5} - \mathbf{R2}) \leq l_1 + l_2 \quad (5)$$

Based on the conditions in (5), the values of the joint variables of mechanism #2 in Table 2 are polished so that

$\mathbf{R1} = (-15, -90)$, $\mathbf{R2} = (-25, 80)$, $\mathbf{R3} = (25, 80)$, $\mathbf{R4} = (10, 90)$ in Table 2 are changed into $\mathbf{R1} = (-51.96, 30)$, $\mathbf{R2} = (-10, 80)$, $\mathbf{R3} = (10, 80)$, $\mathbf{R4} = (51.96, 30)$, respectively. When compared to the original configuration in Table 2, joints R2 and R3 become much closer in the new configuration; hence, four revolute joints R1, R2, R3, and R4 of different link pairs are located very close to each other. Therefore, the actual mechanism for the new configuration should be carefully implemented.

However, another singularity related to joints R2, R3, and R4 occurs, even for the new configuration designed in the previous paragraph. Unlike previous singularities related to joints R5-R1-R2, R4-R5-R3, R3-R5-R4, and R3-R4-R5, in this singularity, the motions of links l_2 and l_3 , connected by joints R2, R3, and R4, cannot be defined by active joints R1 and R5. Fig. 18 describes the moments at which the singularity related to joints R2, R3, and R4 occurs, that is, when (r, θ) are (174 mm, 36°) and (134 mm, 38°), respectively. In order to examine the required joint angles q_1 and q_2 of active joints R1 and R2 and the corresponding wheel rotating speed of modified mechanism #2, an additional simulation to climb up and down the step in Fig. 13 is conducted, and the results are presented in Fig. 19. The trajectory of the wheel center of modified mechanism #2 is the same as that in Fig. 15. First, as shown in Figs. 19(b) and 19(c), there are certain regions, S1, S2, and S3, where the joint angles of R1 and R2 become negative, which implies that the revolute joint changes its rotating direction. Similarly, regions S4, S5, and S6 are observed in Fig. 19(d), where the rotating speed of the wheel becomes negative and changes its moving direction. Moreover, it frequently undergoes drastic changes, which are denoted by cyan blocks. These changes

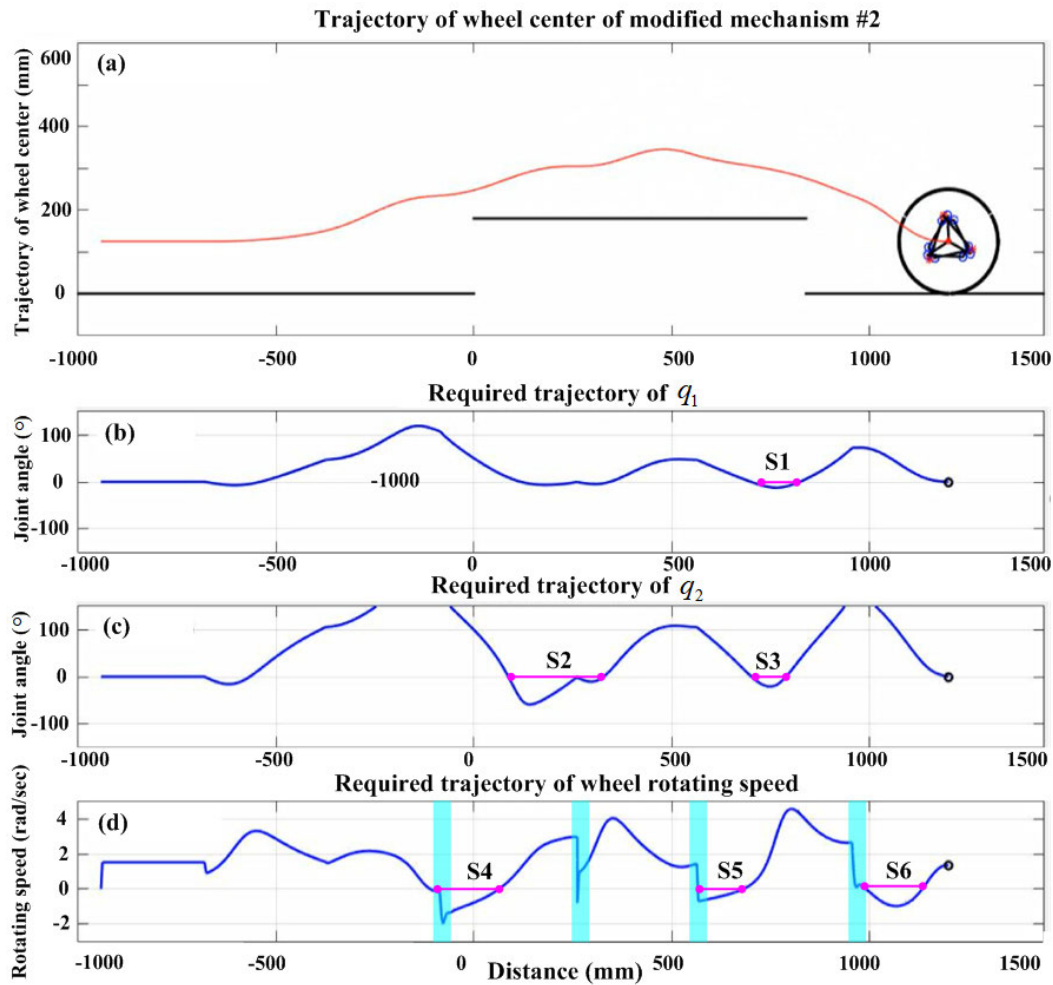


FIGURE 19. (a) Trajectory of the wheel center of modified design alternative #2, (b) and (c) required trajectories of joint angles q_1 and q_2 of R1 and R2, and (d) required trajectory of the wheel rotating speed.

may be a burden because the load capacity and size of the motor used for the revolute joint must be sufficiently large. In summary, mechanism #2 may not be suitable for the proposed 2-DOF shape-morphing wheel mechanism because, as discussed earlier, this mechanism has the largest number of singularities among the five-bar mechanisms of **RRRRR**, **RRRRP**, **PRRRR**, and **PRRRP**. It is worthwhile to note that mechanism #3 also has many revolute joints, four **R**s; hence, it may have singularities similar to those of mechanism #2. In fact, the combination of joints **R3**, **R4**, and **R5** of mechanism #2 in Fig. 6 is a mirror image of the combination of joints **R1**, **R2**, and **R3** of mechanism #3 in Fig. 6.

2) MECHANISM #4

Mechanism #4 is a 3 **R2P** mechanism, with two **P** joints in the wheel base, as shown in Fig. 11(a). In this study, all **P** joints are driven by a rack-pinion mechanism. According to geometric condition in Fig. 20(a), the transformable length of the rack gear is given by $\Delta q = \frac{\sqrt{3}}{2}r$, where

r denotes the wheel radius in the circular configuration. Figs. 20(b) and 20(c) present the values of joint variables q_1 and q_2 of mechanism #4, obtained from the simulation in Fig. 15, respectively. Because the wheel radius r is selected to be 125 mm, the transformable length of the rack gear reaches a maximum of 108.25 mm, which seems sufficient to cover the required transformation ranges for joint variables q_1 and q_2 in Figs. 20(b) and 20(c), respectively.

However, there are two types of interferences during the simulation, as shown in Fig. 21. The first interference between the rack (or rack guide) and step occurs when mechanism #4 lifts its lobe in contact with the ground. To avoid this interference, it is necessary to redesign the trajectory of the wheel center. This center trajectory is optimally determined by minimizing undesired fluctuations while overcoming an obstacle [21]. The second interference between the rack (or rack guide) and wheel lobe occurs immediately after the first interference. One possible solution to this interference is to reduce the length of the wheel lobe; however, as the

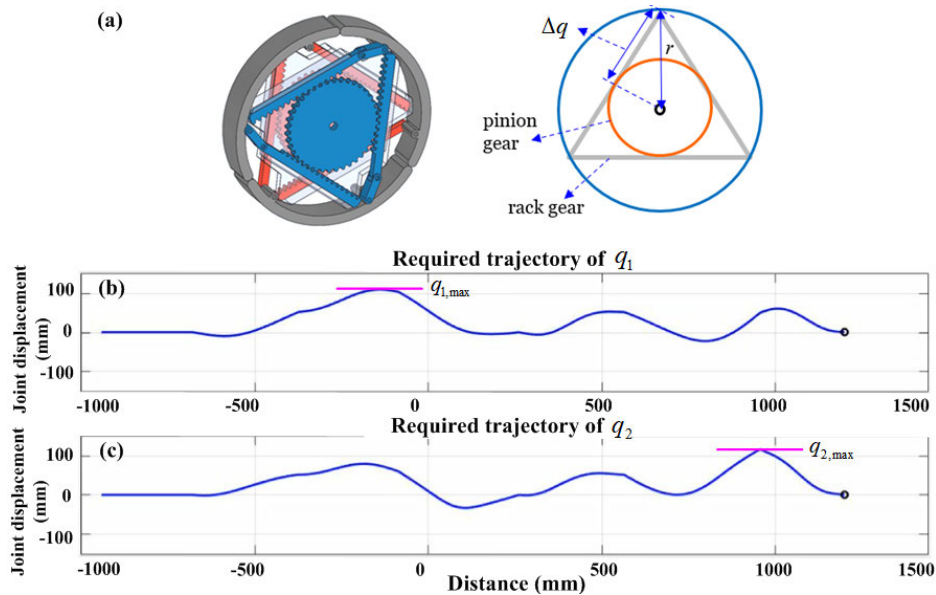


FIGURE 20. (a) Configuration of mechanism #4 and (b) geometric condition.

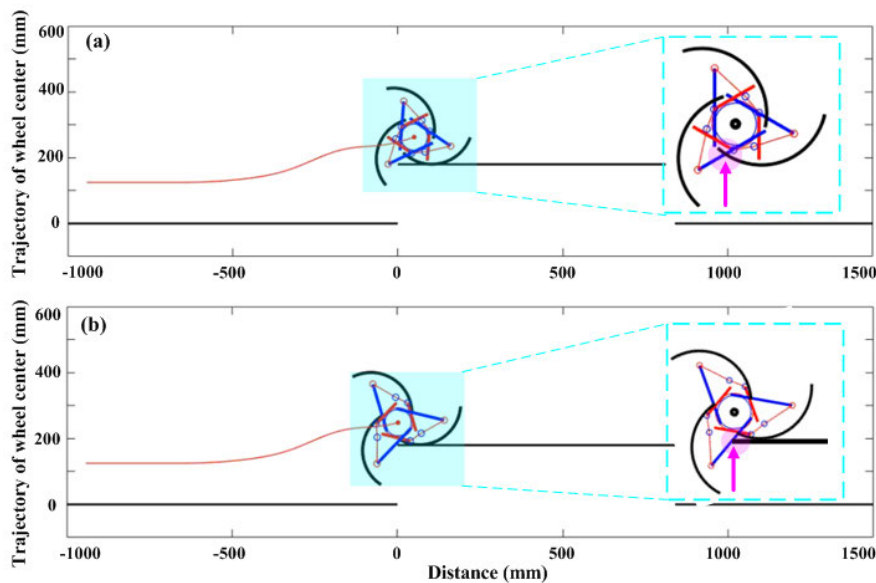


FIGURE 21. Two types of interferences of mechanism #4; between (a) rack and lobe and (b) rack and step.

wheel radius r decreases, the transformable length of the rack gear decreases; as a result, mechanism # 4 cannot cover the required transformation ranges of joint variables q_1 and q_2 .

When compared to mechanism #4, mechanism #5 is free from such interference and can satisfy the required transformation range although it is also based on a 3 **R2P** mechanism with two **P** joints, similar to mechanism #4. The main difference between mechanisms #4 and #5 is the mechanism connecting the lobe. Unlike mechanisms #2 and #3, mechanism #5 has no singularity because for any configuration,

no three **R** joints are located in a straight line. Thus, mechanism #5 is chosen as the final candidate for the proposed 2-DOF shape-morphing wheel mechanism. Fig. 22(a) shows the required trajectories of joint variables q_1 and q_2 corresponding to the displacements of joints **P1** and **P2** for the center trajectory given in Fig. 15. The maximum required trajectories of joint variables q_1 and q_2 of mechanism #5 are smaller than those of mechanism #4. Fig. 22(b) presents the conceptual design of the proposed 2-DOF shape-morphing wheel mechanism, which adopts a four-bar linkage to synchronize the motions of the wheel lobes. The red lines in Fig. 22(a)

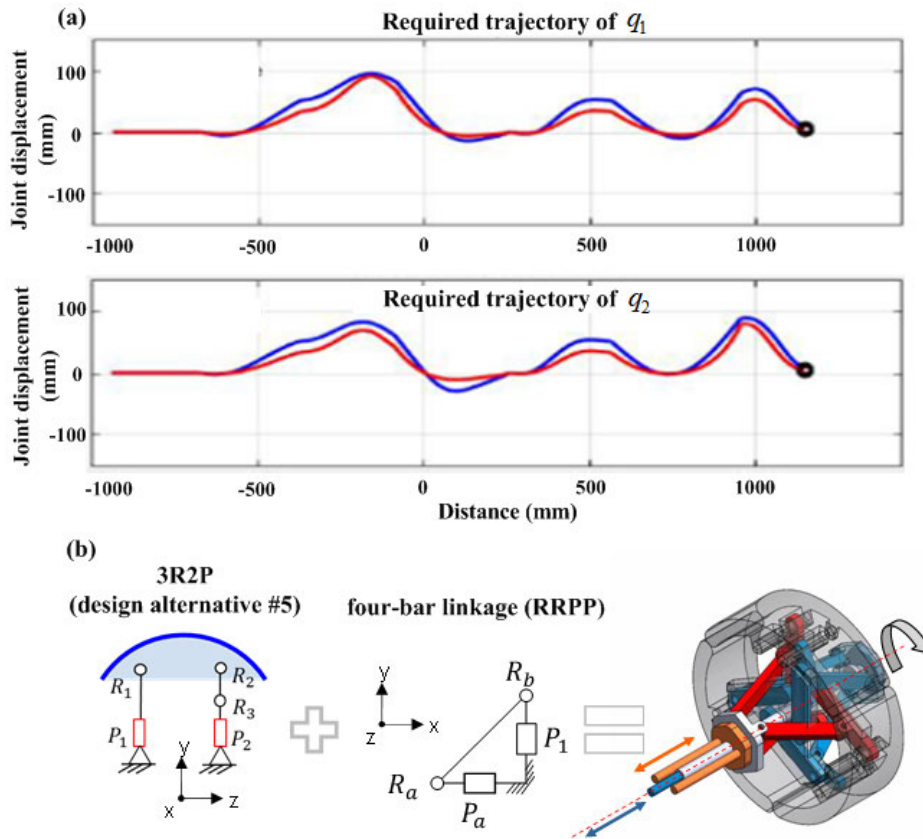


FIGURE 22. (a) Required trajectories of joint variables q_1 and q_2 , and (b) conceptual design of the proposed shape-morphing wheel mechanism based on mechanism #5 combined with four-bar linkage.

denote the displacement of prismatic joint P_a of four-bar mechanism used for the synchronization in Fig. 22(b). For more detailed information regarding the design and manufacturing of the proposed wheel mechanism, please refer to [24].

V. CONCLUSION

In this study, we present the type synthesis of a novel 2-DOF shaping morphing wheel, whose radius and lobe tilting angle can be continuously adjusted to effectively overcome different obstacles. We focus on the process of climbing up and down steps and stairs, which is frequently encountered in indoor environments. Hence, the required transformation ranges of the radius and lobe tilting angle of the proposed wheel are calculated to climb up and down various steps with tread lengths and heights ranging from 260 mm to 340 mm and from 0 mm to 200 mm, respectively. This information plays an important role in transforming the proposed wheel into a desired shape against different steps and stairs. From a kinematic perspective, thirty six 2-DOF mechanisms are searched. Among them, the serial **RR** and parallel **RRRR**, **RRRRP**, **PRRRR**, and **PRRRP** mechanisms are considered as candidates for the proposed 2-DOF shape-morphing mechanism. Through extensive simulations of climbing up and down steps with a height of 180 mm, it is observed that the mechanism with more revolute joints is likely to

have more singularities when three **R** joints are located in a straight line. Here, the motion of the mechanism along the radial or angular direction is restricted, or the joint variables arranged in a row cannot be defined by active joints. In addition, for a **PRRRP** mechanism using the rack-pinion mechanism, interferences between links or between links and the step may occur because of the large length of the rack gear (or guide). To address these difficulties, we chose another **PRRRP** mechanism, combined with ternary links. This mechanism #5 enables tracking of the trajectories of the joint variables to satisfy the required wheel transformation without any singularity or interference. Based on this mechanism, we implement the proposed 2-DOF motions of the shape-morphing wheel mechanism successfully.

REFERENCES

- [1] M. Kim, S. Kim, S. Park, M.-T. Choi, M. Kim, and H. Goma, "Service robot for the elderly," *IEEE Robot. Autom. Mag.*, vol. 16, no. 1, pp. 34–45, Mar. 2009.
- [2] C. Jayawardena, I. H. Kuo, U. Unger, A. Igic, R. Wong, C. I. Watson, R. Q. Stafford, E. Broadbent, P. Tiwari, J. Warren, and J. Sohn, "Development of a service robot to help older people," in *Proc. IEEE/RSJ Int. Conf. Intell. Robots Syst.*, Oct. 2010, pp. 5990–5995.
- [3] C.-J. Lin, T.-H.-S. Li, P.-H. Kuo, and Y.-H. Wang, "Integrated particle swarm optimization algorithm based obstacle avoidance control design for home service robot," *Comput. Electr. Eng.*, vol. 56, pp. 748–762, Nov. 2016.

- [4] M. Wise, M. Ferguson, D. King, E. Diehr, and D. Dymesich, "Fetch and freight: Standard platforms for service robot applications," in *Proc. Workshop Auton. Mobile Service Robots*, Jul. 2016, pp. 1–6.
- [5] T. Yamamoto, K. Terada, A. Ochiai, F. Saito, Y. Asahara, and K. Murase, "Development of human support robot as the research platform of a domestic mobile manipulator," *ROBOMECH J.*, vol. 6, no. 1, pp. 1–15, Dec. 2019.
- [6] D. Choi, Y. Kim, S. Jung, J. Kim, and H. S. Kim, "A new mobile platform (RHymO) for smooth movement on rugged terrain," *IEEE/ASME Trans. Mechatronics*, vol. 21, no. 3, pp. 1303–1314, Jun. 2016.
- [7] D. Kim, H. Hong, H. S. Kim, and J. Kim, "Optimal design and kinetic analysis of a stair-climbing mobile robot with rocker-bogie mechanism," *Mechanism Mach. Theory*, vol. 50, pp. 90–108, Apr. 2012.
- [8] D. Choi, Y. Kim, S. Jung, H. S. Kim, and J. Kim, "Improvement of step-climbing capability of a new mobile robot RHymO via kineto-static analysis," *Mechanism Mach. Theory*, vol. 114, pp. 20–37, Aug. 2017.
- [9] U. Saranlı, M. Buehler, and D. E. Koditschek, "RHex: A simple and highly mobile hexapod robot," *Int. J. Robot. Res.*, vol. 20, no. 7, pp. 616–631, Jul. 2001.
- [10] V. Klemm, A. Morra, C. Salzmann, F. Tschopp, K. Bodie, L. Gulich, N. Kung, D. Mannhart, C. Pfister, M. Vierneisel, F. Weber, R. Deuber, and R. Siegwart, "Ascento: A two-wheeled jumping robot," in *Proc. Int. Conf. Robot. Autom. (ICRA)*, May 2019, pp. 7515–7521.
- [11] Y.-S. Kim, G.-P. Jung, H. Kim, K.-J. Cho, and C.-N. Chu, "Wheel transformer: A wheel-leg hybrid robot with passive transformable wheels," *IEEE Trans. Robot.*, vol. 30, no. 6, pp. 1487–1498, Dec. 2014.
- [12] S.-C. Chen, K.-J. Huang, W.-H. Chen, S.-Y. Shen, C.-H. Li, and P.-C. Lin, "Quattroped: A leg-wheel transformable robot," *IEEE/ASME Trans. Mechatronics*, vol. 19, no. 2, pp. 730–742, Apr. 2014.
- [13] W.-H. Chen, H.-S. Lin, Y.-M. Lin, and P.-C. Lin, "TurboQuad: A novel leg-wheel transformable robot with smooth and fast behavioral transitions," *IEEE Trans. Robot.*, vol. 33, no. 5, pp. 1025–1040, Oct. 2017.
- [14] D. Y. Lee, J. S. Kim, J. J. Park, S. R. Kim, and K. J. Cho, "Fabrication on origami wheel using pattern embedded fabric and its application to a deformable mobile robot," in *Proc. IEEE Int. Conf. Robot. Autom.*, Jun. 2014, p. 2565.
- [15] D.-Y. Lee, J.-S. Koh, J.-S. Kim, S.-W. Kim, and K.-J. Cho, "Deformable-wheel robot based on soft material," *Int. J. Precis. Eng. Manuf.*, vol. 14, no. 8, pp. 1439–1445, Aug. 2013.
- [16] V. Kucherenko, A. Bogatchev, and M. VanWinnendael, "Chassis concepts for the ExoMars rover," in *Proc. 8th ESA Workshop Adv. Space Technol. Robot. Automat.*, Noordwijk, The Netherlands, Nov. 2004, pp. 1–8.
- [17] R. Siegwart, P. Lamon, T. Estier, M. Lauria, and R. Piguët, "Innovative design for wheeled locomotion in rough terrain," *Robot. Auto. Syst.*, vol. 40, nos. 2–3, pp. 151–162, Aug. 2002.
- [18] D. Choi, J. R. Kim, S. Cho, S. Jung, and J. Kim, "Rocker-pillar: Design of the rough terrain mobile robot platform with caterpillar tracks and rocker bogie mechanism," in *Proc. IEEE/RSJ Int. Conf. Intell. Robots Syst.*, Oct. 2012, pp. 3405–3410.
- [19] K. Sasaki, Y. Eguchi, and K. Suzuki, "Step-climbing wheelchair with lever propelled rotary legs," in *Proc. IEEE/RSJ Int. Conf. Intell. Robots Syst. (IROS)*, Sep. 2015, pp. 6354–6359.
- [20] F. Guo, S. Wang, and J. Wang, "A search-based control architecture for wheel-quadruped robot obstacle negotiation," in *Proc. Annu. Amer. Control Conf. (ACC)*, Jun. 2018, pp. 2231–2236.
- [21] K. Kim, Y. Kim, J. Kim, H. S. Kim, and T. Seo, "Optimal trajectory planning for 2-DOF adaptive transformable wheel," *IEEE Access*, vol. 8, pp. 14452–14459, 2020.
- [22] *The Stairway Manufacturing Code Association*, Int. Residential Code, Dalton, OH, USA, 2006.
- [23] J. J. Cervantes-Sánchez and J. G. Rendón-Sánchez, "A simplified approach for obtaining the workspace of a class of 2-dof planar parallel manipulators," *Mechanism Mach. Theory*, vol. 34, no. 7, pp. 1057–1073, Oct. 1999.
- [24] Y. Kim, Y. Lee, S. Lee, J. Kim, H. S. Kim, and T. Seo, "STEP: A new mobile platform with 2-DOF transformable wheels for service robots," *IEEE/ASME Trans. Mechatronics*, vol. 25, no. 4, pp. 1859–1868, Aug. 2020.



YOUNGSOO KIM received the B.S. and Ph.D. degrees in mechanical and aerospace engineering from Seoul National University, in 2013 and 2019, respectively. His research interests include service robot design, mobile mechanism design, and optimization.



HWA SOO KIM (Member, IEEE) received the B.S. and Ph.D. degrees in mechanical engineering from Seoul National University, South Korea, in 2000 and 2006, respectively. He is currently a Professor with the Department of Mechanical System Engineering, Kyonggi University. His current research interests include design, modeling, and control of various mobile platforms for wall-cleaning and stair-climbing.



TAEWON SEO (Senior Member, IEEE) received the B.S. and Ph.D. degrees from the School of Mechanical and Aerospace Engineering, Seoul National University, South Korea. He is currently an Associate Professor with the School of Mechanical Engineering, Hanyang University, South Korea. His research interests include robot design, analysis, control, optimization, and planning. He received the Best Paper Award of the IEEE/ASME TRANSACTIONS ON MECHATRONICS, in 2014. He is working as a Technical Editor of IEEE/ASME TRANSACTIONS ON MECHATRONICS. He is working as an Associate Editor of IEEE ROBOTICS AND AUTOMATION LETTERS and *Intelligent Service Robotics*.

...